# IMAGE RESTORATION FOR RESOLUTION IMPROVEMENT OF DIGITAL AERIAL IMAGES: A COMPARISON OF LARGE FORMAT DIGITAL CAMERAS

S. Becker[1], N. Haala[1], E.Honkavaara[2], L. Markelin[2]

[1]Universitaet Stuttgart, Institute for Photogrammetry, Germany – (susanne.becker, norbert.haala)@ifp.uni-stuttgart.de
[2]Finnish Geodetic Institute, Geodeetinrinne 2, FIN-02430 Masala, Finland – (eija.honkavaara, lauri.markelin)@fgi.fi

**Commission I, WG I/4**

**KEY WORDS:** geometry, calibration, high resolution, spatial, performance

**ABSTRACT:**
Within the paper a comparative quantification of the spatial image resolution for large-format digital airborne cameras will be presented. For this purpose, imagery of the Leica ADS40, the Intergraph Z/I-imaging DMC and the Vexcel UltraCamD were examined. The respective spatial resolutions are represented by means of the point spread function, which can be measured easily and reliably at image edges. Thus, images of test patterns like a Siemens star were used. In addition to the evaluation of the original images as they are provided by the camera systems, the potential benefit of a resolution improvement by image restoration is demonstrated. Therefore, a linear restoring finite impulse response filter is applied. Usually, colour image acquisition by digital aerial camera systems is realised by combining data from the multi-spectral module with higher resolution panchromatic imagery. The quality of this pan-sharpening process is presented in the final part of the paper. For this purpose, the potential degradation of colour information by this process was quantified for the three tested camera systems in addition to the resolution measurements.

## 1. INTRODUCTION

Spatial resolution is one of the most important parameters in the context of aerial image acquisition. Traditionally, it is specified by the ground sampling distance (GSD), which is computed by projecting the pixel size from the camera's focal plane to the ground. This parameter is not very expressive in the context of digital large-format airborne cameras. It relates to raw imagery while such high-end systems usually provide pre-processed imagery for photogrammetric processing. As an example, multi-head systems like the Intergraph/ZI-Imaging DMC and the Vexcel UltracamD combine smaller format images from single staring arrays to large format 'virtual' images. Alternatively, a large field of view and a high geometric resolution are based on the application of CCD-line sensors like it is for example realised by the Leica ADS40. Such systems are subject to image distortions from high frequency movement, which requires a rectification of the raw image strips to a reference surface.

All these geometrical transformations adulterate the original value of the GSD. One alternative approach to determine the spatial resolution of such pre-processed images is to measure the size of the smallest details, which can be identified by a human operator. However, the required human interpretation limits the objectivity of such results. For these reasons, the spatial resolution of the different imaging systems is described in terms of the point spread function (PSF). As it will be discussed in section 2.1 the PSF can be measured easily at image edges, which are either provided from a test pattern like a Siemens star or from natural structures. Section 2.2 gives a brief introduction into our approach on image restoration, which is additionally used to improve the resolution of the investigated imagery. Within section 3 the results of resolution quantification are given for the camera systems ADS40 from Leica Geosystems, the DMC from Intergraph and the Vexcel UltraCamD. In addition to the evaluation of the original images, as they are provided from the camera vendors, the potential resolution improvement by the approach discussed in section 2.2 will be demonstrated. While section 3 gives the results for the panchromatic imagery of the investigated systems, within section 4 the resolution of the multispectral data is quantified. Usually, pan-sharpening algorithms are applied to enhance the multispectral images by the higher resolution panchromatic data. While these algorithms can generate multispectral data at the resolution of the panchromatic images, their original colours are potentially falsified. Thus, in addition to the quantification of the spatial resolution improvement, the preservation of colour values is evaluated in this section, additionally. Finally, the pan-sharpening, as it is implemented by the camera vendors, is compared to the result of our algorithm.

## 2. IMAGE RESOLUTION: EVALUATION AND IMPROVEMENT

Besides additive noise, image resolution is mainly limited by blur, which occurs in any imaging system that uses electromagnetic radiation. Blurring results from atmospheric distortions or relative motion of the depicted objects. However, the most common degradations are caused by imperfections of the sensors or transmissions. The quality of the optical system is restricted by defocusing or the limited spatial extent of the aperture, lenses and mirrors. Image degradation also results during discretization since an averaged illumination is measured for each CCD detector.

### 2.1 Measurement of image degradation

The blur of the system is generally characterized by the PSF or impulse response, which can therefore be used very well to describe the resolution of an imaging system. The PSF can be measured without problems at image edges, which are either provided from test patterns or from natural structures. A convenient approach to objectively quantify image resolution is the analysis of radial modulation of the Siemens star. As it can be seen in the left part of Figure 1, grey values are measured along circles. The right part of Figure 1 presents the measured grey values for one circle exemplarily. Different diameters realise variable spatial frequencies. The evaluation of the modulation for different radii gives a quantitative prediction for the resolution.

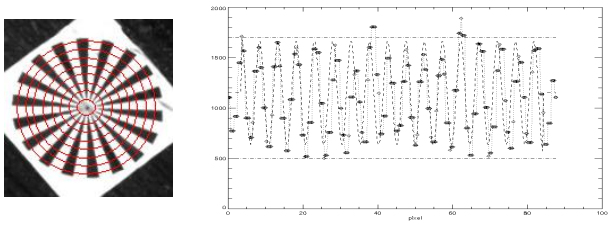

Figure 1. Radial modulation analysis for one circle of the Siemens star

The measured maximal and minimal grey values $I_{min}, I_{max}$ allow the computation of the modulation depth

$$M = \frac{I_{max} - I_{min}}{I_{max} + I_{min}} \quad (1)$$

for each frequency. As i.e. described in (Boremann 2001) these values are then used to determine the modular transfer function (MTF). Since the MTF can be modelled by a Gaussian shape function, it is specified by $\sigma_{MTF}$ and thus can be linked by

$$\sigma_{PSF} = \frac{1}{2\pi\sigma_{MTF}} \quad (2)$$

to the corresponding PSF (Jahn et al, 1995). In the following $\sigma_{PSF}$ is used to compare the resolution of different camera systems.

### 2.2 Image restoration

The resolution of an image can be further improved by image restoration, which aims on recovering the original scene from the degraded image observations. By these means, image restoration estimates an inverse filter to compensate for image degradations, including random noise and blurring. Since this process is an ill-posed problem, there is no unique solution and a small amount of noise can result in large reconstruction errors. Therefore, restoration methods aim at modelling the degradation by using a priori knowledge of the original scene and PSF as well as noise information. The method which is used within this paper is the linear restoring impulse response (FIR) filter (Saleh et al, 1983). It is based on the estimation

$$\hat{I}_{i,j} = \sum_{k,l} a_{k,l} \cdot I'_{i-k,j-l} \quad (3)$$

of the original scene using the actually measured intensity values $I'_{(i,j)}$ and the filter coefficients $a_{k,l}$. The FIR filter minimizes the average mean-square error

$$\Im(a) = \left\langle \left[ \hat{I}_{i,j} - I_{i,j} \right]^2 \right\rangle \quad (4)$$

between the estimated signal $\hat{I}_{(i,j)}(x,y)$ and the original scene $I_{(i,j)}(x,y)$. For this purpose, the optimal filter coefficients of equation (3) are determined by a least mean square solution. The FIR filter approach is a local algorithm that assumes the noise to be zero-mean and white. Its probability function is a Gaussian distribution with standard deviation $\rho$. The original scene is expected to be a stationary random process with a Gaussian probability function and standard deviation $\kappa$. This kind of a priori knowledge is necessary for the stabilisation of the reconstruction problem. It can be controlled with the regularisation parameter $\varepsilon^2=\rho^2/\kappa^2$ that includes both information on the noise and the scene.

### 2.3 Selected parameters and restoration results

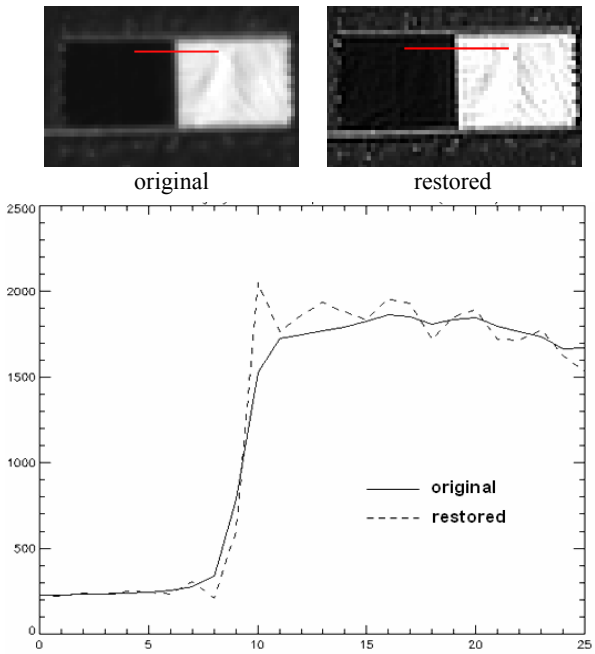


Figure 2. Grey value profiles before and after image restoration

The effect of image restoration on edges and homogeneous areas is illustrated in Figure 2. As it is visible on the top row of the figure, the restored image on the right appears sharper than the original image on the left, while the noise increases. These effects are verified by the grey value profiles depicted in the bottom of Figure 2. The profiles were extracted along the red line from the respective images before and after image restoration. While image restoration enhances the edge, homogeneous grey value areas become noisier.

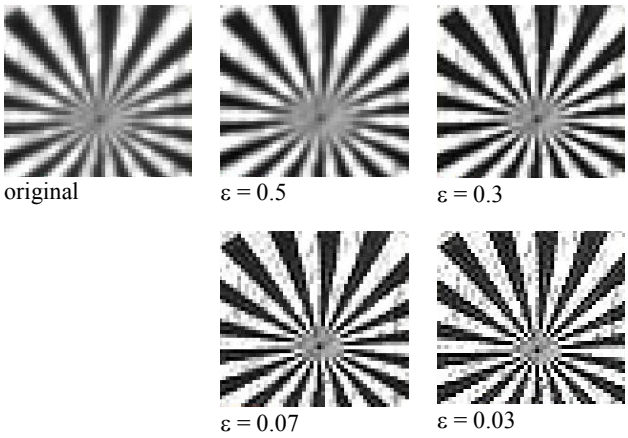


Figure 3. Result of restoration algorithm for $\rho$=0.8 and different $\varepsilon$ values (with filter size $m$=5)

The amount of the resolution improvement and the corresponding increase in noise of the FIR filter approach depends on the selected value of the regularisation parameter $\varepsilon$. The influence of different $\varepsilon$ values on the restoration result is demonstrated exemplarily in Figure 3. As it is visible for the example for $\varepsilon$=0.5, large values of $\varepsilon$ result in a smoothing effect. In contrast, the restored images for $\varepsilon$=0.07 and $\varepsilon$=0.03 show that small values improve the visible resolution but increase the noise.

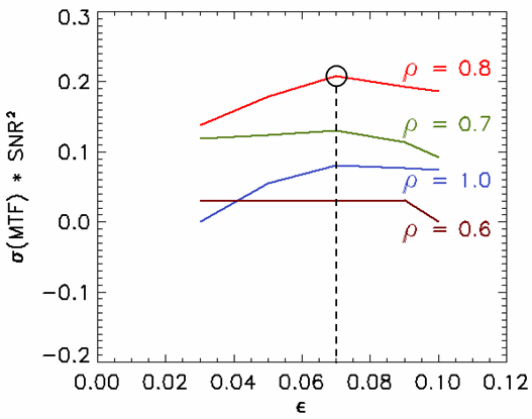


Figure 4. Resolution and SNR as function of the $\varepsilon$ value

The optimal restoration parameters $\varepsilon$ and $\rho$ can be found by means of an appropriate system performance metric that considers both resolution and sensitivity measures. For this purpose, a figure of merit (FOM) is designed from the product of the $\sigma_{MTF}$ and the squared signal to noise ratio (SNR). The best parameter combination is defined by the maximum of the FOM. As an example, Figure 4 gives the FOM for a DMC data set with GSD=8cm. Its maximum is achieved for the parameters $\rho$=0.8 and $\varepsilon$=0.07. These values turned out to be quite constant even for various flying heights and acquisition periods. A number of additional tests based on UltraCamD and ADS40 data showed very similar results. For this reason, the above mentioned restoration parameters were used for all three digital camera systems investigated in our paper.

## 3. RESOLUTION MEASUREMENTS

Within our tests imagery from the ADS40 of Leica Geosystems (Sandau et al 2000), the DMC from Intergraph (Hinz et al 2000) and the Vexcel UltraCamD (Leberl F. et al 2003) were evaluated. Originally, the ADS40 imagery was collected during a test on the potential improvement of spatial resolution by staggered arrays (Reulke et al 2004) (Becker et al 2005). Such staggered images are optionally collected for each pan-chromatic channel by two parallel CCD lines which are shifted by half a pixel. Thus, panchromatic data is collected in the forward, nadir and backward view by two 12k pixel CCD line arrays with a pixel size of 6.5µm. However, in this paper imagery collected in the non-staggered configuration by single CCD lines is investigated exemplarily. For the evaluated flying height of 1500m the pixel size of 6.5µm and the focal length of 62.77mm resulted in a nominal GSD of 15.5cm.

While the ADS40 data was collected in Vaihingen/Enz near Stuttgart, the UltraCamD and the DMC imagery was captured at the Sjökulla test-field of the Finnish Geodetic Institute. A detailed description of the test configuration can be found in (Honkavaara et al 2005) and (Honkavaara et al 2006). In this paper data from a flying height of 800m for the DMC and 900m for the UltraCamD was investigated. During pre-processing of the DMC data a 'virtual' 8kx13k DMC image is generated from four synchronously captured sub-images. Since these images have a pixel size of 12µm and a focal length of 120mm, these parameters are also used for generation of the virtual image. This resulted in a nominal GSD of 8cm for our configuration.

Data from four camera heads is also combined during pre-processing of the panchromatic UltraCamD imagery. Each of these four camera modules has the same field-of-view, but has its CCDs placed in a different position in the focal plane. By these means a set of 9 sub-images with a physical pixel size of 9µm and a focal length of 100mm is captured. These sub-images are then combined to a virtual image with the same nominal parameters. This again resulted in a nominal GSD of 8cm for our UltraCamD imagery.

Finally, analogue images of a RC20 camera were evaluated, which were captured simultaneously with the UltraCamD data. In order to provide approximately the same image width in ground as UltraCamD, intermediate angle optic (214mm) was used. Since the analogue images were scanned at a resolution of 20µm, the GSD again was 8cm.

| | flight direction | $\sigma_{PSF}$ (original) | $\sigma_{PSF}$ (restored) |
|---|---|---|---|
| DMC (GSD=8cm) | along track | 0.40 pix | 0.26 pix |
| | cross track | 0.39 pix | 0.26 pix |
| UltraCamD (GSD=8cm) | along track | 0.48 pix | 0.35 pix |
| | cross track | 0.47 pix | 0.32 pix |
| ADS40 (GSD=15cm) | along track | 0.52 pix | 0.44 pix |
| | cross track | 0.65 pix | 0.49 pix |
| RC20 (GSD=8cm) | along track | 0.38 pix | 0.31 pix |
| | cross track | 0.38 pix | 0.30 pix |

Table 1. $\sigma_{PSF}$ of original and restored panchromatic image data

The resolution quantification for the different camera systems by measurement of the point spread function at a Siemens star is given in Table 1. While the third column gives the $\sigma_{PSF}$ of the original panchromatic data, as it is provided by the camera vendors, the final column gives $\sigma_{PSF}$ after image restoration. As it was already discussed in section 2.3, the restoration of the DMC, UltraCamD and ADS40 images is based on the optimal filter parameters $\rho$=0.8 and $\varepsilon$=0.07. For the RC20 data the optimal restoration values were empirically found to be $\rho$=0.6 and $\varepsilon$=0.1. This most likely reflects some higher degree of noise in the RC20 images. In order to detect potential effects of motion blur for the frame based systems, the resolution was also determined both along and cross track direction. For this purpose the resolution measurement was limited to image regions depicting suitable sections of the Siemens star. As it is visible, the time delayed integration which is applied by DMC and UltraCamD, as well as the forward motion compensation of the RC20, leads to almost similar resolution results for both directions. However, for other evaluations the resolution cross track was found to be slightly better than along track for DMC and UltraCamD, and vice versa for RC20 (Honkavaara et al, 2005) (Honkavaara et al, 2006). By contrast, the resolution of the ADS40 data is significantly better along track than cross track. This is due to the fact that the data was acquired in staggered array mode. Thus, the point sampling distance in flying direction was half of the sampling distance in cross direction for each panchromatic line. Since each of the $\sigma_{PSF}$ values is determined from one exemplary data set, they should not be regarded as being general, though. Nevertheless, the quantitative improvement of spatial resolution by image restoration is quite constant, referring to the digitally acquired data sets. The average resolution enhancement is of about 28% for DMC, UltraCamD and ADS40 images.

To further demonstrate the influence of image restoration, the MTF before and after restoration is exemplarily plotted for a

UltraCamD data set in Figure 5. The measurements of the MTF at different radii of the Siemens star are depicted by circles and crosses, representing measures in the original and the restored image, respectively. Based on these measures the corresponding Gaussian shape function was estimated. As it is visible, the single MTF measures are noise prone especially for the restored image. However, the improved resolution is still clearly visible.

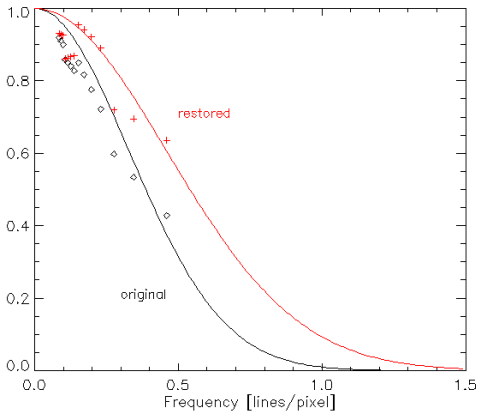


Figure 5. MTF of original and restored UltraCamD image data

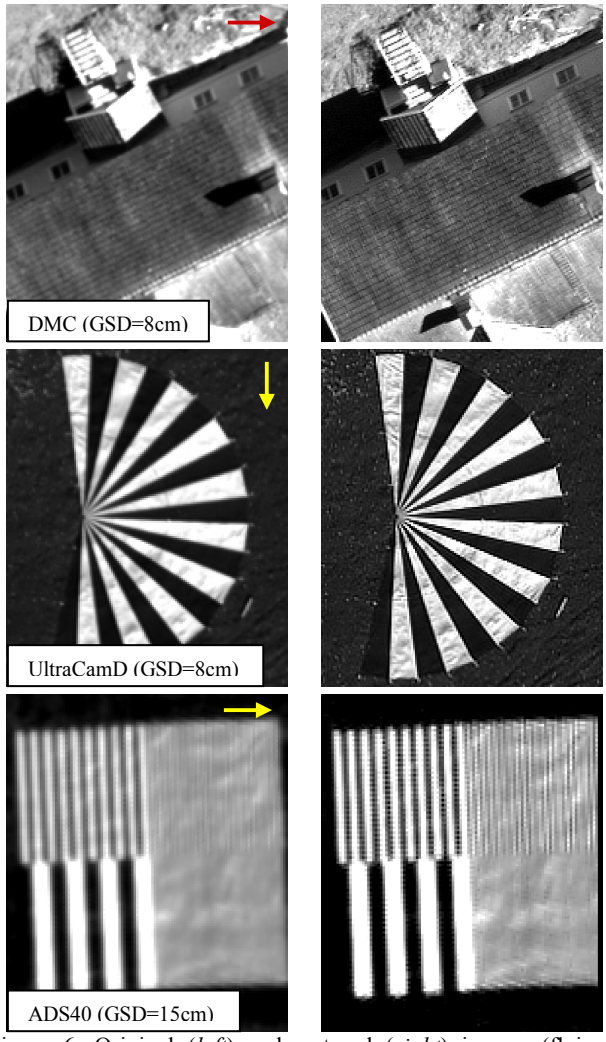


Figure 6. Original (*left*) and restored (*right*) images (flying direction marked by arrows in left images)

The improved resolution is also clearly visible in exemplary images of the different camera systems in Figure 6. After restoration image structures appear sharper and the visibility of even small details like the tiles in the DMC image is improved.

## 4. PAN-SHARPENING

In the preceding section resolution quantification and improvement was demonstrated for panchromatic images. However, these techniques can also be used for the processing of multispectral images. Usually, digital aerial cameras collect these multispectral images at a smaller spatial resolution than the panchromatic data. In a post-processing step, pan-sharpening algorithms are then used to generate multispectral data at a resolution that is comparable to the resolution of the corresponding panchromatic images by combining both data sources. This approach has been used for satellite images for many years, thus several algorithms are available. According to their design, these methods can be classified for example in substitution approaches, arithmetic and filter based techniques. In the following, representative methods of each class are briefly introduced and validated, subsequently. Substitution methods are characterised by the replacement of the structural component of the multispectral image with the panchromatic image data (Bretschneider et al, 2000). Prior to this substitution, the structural information of the multispectral data must be extracted. Well-known approaches based on the substitution method are the IHS (Intensity, Hue, Saturation) - and HSV (Hue, Saturation, Value) - transformation and the PCA (Principal Components Analysis) (Zhang, 2002) (Gonzalez et al, 1992). The principle of the arithmetic methods consists in merging panchromatic and multispectral grey values by means of arithmetic operations like addition, subtraction, multiplication and division (Pohl et al, 1998). One member of this class of algorithms is given by the Brovey transformation (Vrabel, 1996). The concept of the filter-based techniques is to eliminate the spatial structures from the panchromatic image with the help of filters and add them to the multispectral data (Gonzalez et al, 1992). Depending on the filter characteristics various approaches can be distinguished.

### 4.1 Resolution improvement

In our investigations the resolution improvement was determined for all these different pan-sharpening algorithms. Additionally, the approaches were tested for two scenarios: pan-sharpening based on the original and the restored panchromatic image. As in section 3, the panchromatic data was restored by the FIR filter approach with the optimal filter parameters $\rho$=0.8 and $\varepsilon$=0.07.

| | flight direct. | $\sigma_{PSF}$ (orig.) | $\sigma_{PSF}$ (IHS with orig. pan) | $\sigma_{PSF}$ (IHS with rest. pan) |
|---|---|---|---|---|
| DMC (GSD=8cm) | along | 1.73 pix | 0.49 pix | 0.29 pix |
| | cross | 1.68 pix | 0.44 pix | 0.24 pix |
| UltraCamD (GSD=8cm) | along | 1.52 pix | 0.57 pix | 0.39 pix |
| | cross | 1.42 pix | 0.55 pix | 0.33 pix |
| ADS40 (GSD=15cm) | along | 0.78 pix | 0.60 pix | 0.51 pix |
| | cross | 0.76 pix | 0.66 pix | 0.59 pix |

Table 2. $\sigma_{PSF}$ for original and pan-sharpened multispectral images, values refer to the corresponding size of the panchromatic pixels

For the ADS40 the focal length and pixel size is equal for the multispectral and the non-staggered panchromatic imagery. Thus, the resolution improvement by pan-sharpening is limited. In contrast, the focal length changes from 28mm for the multispectral module to 100mm for the panchromatic (ratio 1:3.6) of the UltraCamD. Similarly, the value changes from 25mm to 120mm (ratio 1:4.8) for the DMC. Thus, considerable differences in resolution are present in the collected images, resulting in a significant effect of the pan-sharpening process. This resolution improvement was again quantified by MTF analysis. Since very similar results were achieved for all the tested algorithms, the PSF values $\sigma_{PSF}$ are given exemplarily for the IHS method in Table 2. The respective values $\sigma_{PSF}$ refer to the size of the corresponding panchromatic pixels. As it is visible, pan-sharpening based on original panchromatic data reduces the $\sigma_{PSF}$ values of the multispectral bands clearly. However, they are still significantly higher than the $\sigma_{PSF}$ values of the corresponding panchromatic images depicted in Table 1. If restored panchromatic images are used, the image resolution is additionally increased by approximately 30%. Consequently, the resulting spatial resolution of the multispectral data is better than the one of the corresponding original pan-images and even almost as good as the resolution of the restored pan-data. Figure 7 shows pan-sharpening results exemplarily for the IHS approach. The resolution enhancement that can be achieved by applying a pan-sharpening with the original panchromatic image is obvious. Further improvement is visible if restored panchromatic data is used. Grey value edges seem to be sharper and the visibility of small image structures is increased.

### 4.2 Colour preservation

Pan-sharpening algorithms aim at the resolution improvement of multispectral images while preserving their original colour values. Good colour preservation is especially important if a spectral analysis like classification is aspired in subsequent steps. In order to improve the colour preservation of the tested pan-sharpening methods, a histogram matching was applied. In this pre-processing step the histogram of the panchromatic image is adapted to the histogram of the intensity image which can be derived from the multispectral bands. The quantification of a potential change of colour values requires the definition of an appropriate colour space. As an example, colour differences in the CIE-L*a*b* colour space correspond to the differences as they are perceived by the human eye (Becker et al, 2005). However, for reasons of simplicity, the original colour spaces of the respective pan-sharpening approaches were used to quantify the relative amount of colour degradation.

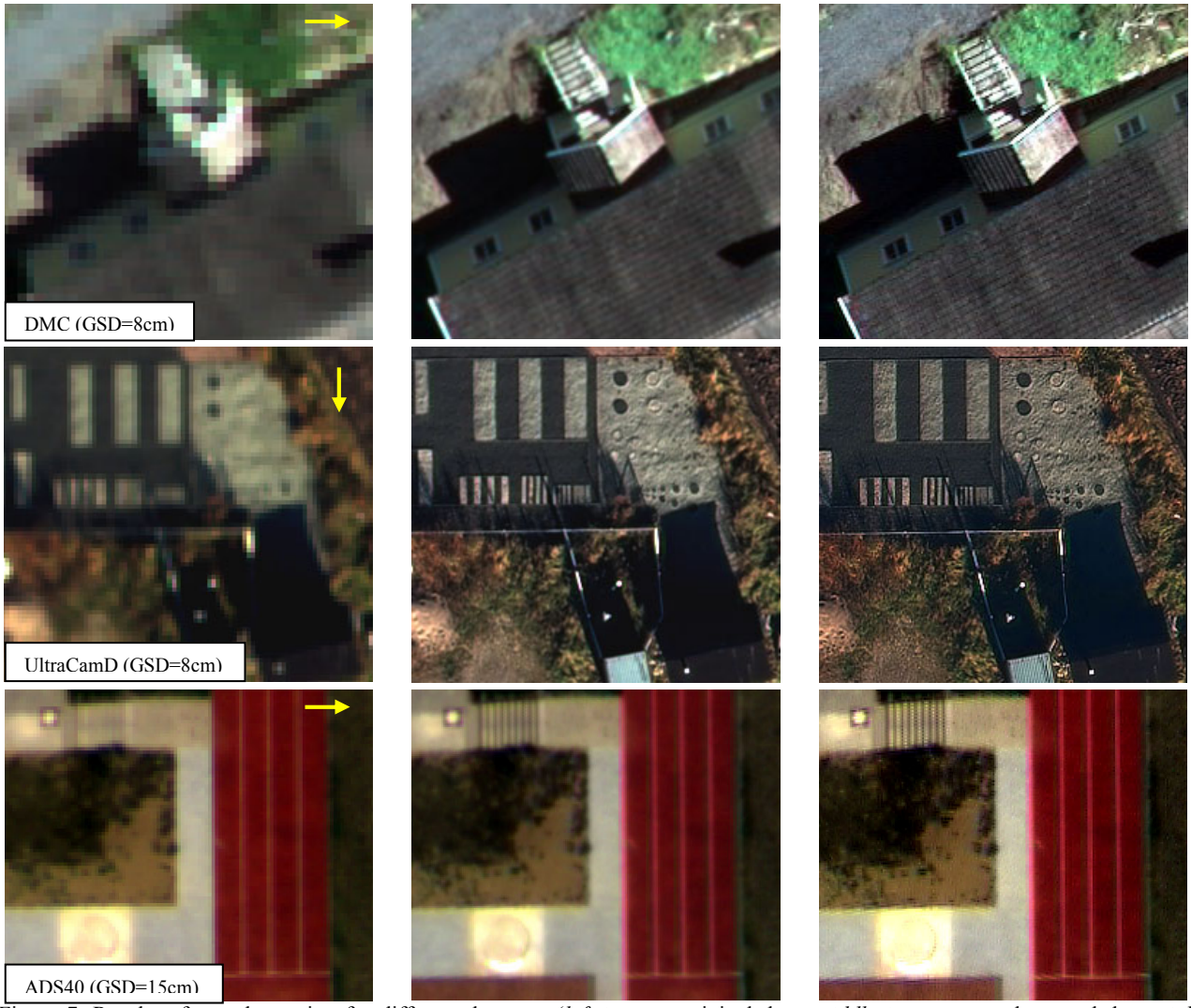


Figure 7. Results of pan-sharpening for different data sets (*left images:* original data, *middle images:* pan-sharpened data, *right images:* pan-sharpened data based on restored pan-images), flying direction marked by arrows in left images

To determine the degradation of colour information, the pan-sharpened images were compared to the low-resolution multispectral data. However, different radiometric resolutions of the camera systems hinder a comparison based on absolute difference values. Therefore, the colour distortion values are compared to the colour deviations of the pan-sharpening products that can be generated with the cameras' standard post-processing software. These vendor provided software tools use a YIQ and HSV approach, which is based on a modified definition of colour space with respect to the IHS approach used in section 4.1.

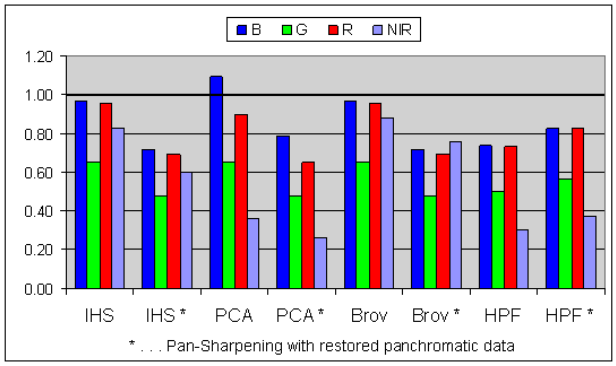


Figure 8. Relative colour deviations for UltraCamD data

Figure 8 exemplarily depicts the respective colour distortions in the pan-sharpened multispectral bands for UltraCamD data. For the pan-sharpening results the average DN differences of each band are divided by the corresponding DN differences of the pan-sharpened images generated by the vendors' standard software. Thus, values smaller than 1.0 mean, that the colour preservation is better than in the vendors' products. As it can be seen in Figure 8, the tested pan-sharpening methods perform well. Even if restored panchromatic images are used, the colour distortions remain small compared to the standard pan-sharpening products. Analogous analyses with image data of the other camera systems showed very similar results. This confirms that the use of restored panchromatic data yields an additional improvement of spatial resolution while not leading to significant additional colour distortions.

## 5. CONCLUSIONS

Within the paper, the spatial resolution of the digital aerial cameras Leica ADS40, the Intergraph Z/I-imaging DMC and the Vexcel UltraCamD was determined by objective measurements at suitable test patterns. Additionally, the beneficial effect of image restoration and pan-sharpening could be quantified. Despite the fact that the resolution of the different cameras was quantified using suitable measures, it has to be emphasized, that our tests do not yet allow for a direct comparison or even ranking of the different systems. Each flight was performed with different configurations and in different conditions. Additionally, some effects like the dependency of the image resolution from camera movement or the relative position of the resolution pattern within the virtual full frame image have to be investigated in more extensive tests. Finally, as it can be seen for the scanned RC20 images, which have a resolution comparable to the digital cameras, but a much lower signal-to-noise-ratio, the quality of aerial images depends on a number of different parameters.

## REFERENCES


Becker, S., Haala, N., Reulke, R., 2005. Determination and Improvement of Spatial Resolution for Digital Aerial Images. ISPRS Workshop: High-Resolution Earth Imaging for Geospatial Information, Hannover, Germany.

Boreman, G., 2001. *Modulation Transfer Function in Optical and Electro-Optical Systems*. SPIE - The International Society for Optical Engineering, Bellingham, Washington, USA.

Bretschneider, T., Kao, O., 2000. Image Fusion in Remote Sensing. Proceedings of the 1st Online Symposium of Electronic Engineers.

Gonzalez, R.C., Woods, R.E., 1992. *Digital Image Processing*. Reading, Mass.: Addison-Wesley.

Hinz, A., Dörstel, C., Heier, H., 2000. Digital Modular Camera: System Concept and Data Processing Workflow. *IAPRS*, Vol 33, Part B2, pp.164-171.

Honkavaara, E., Jaakkola, J., Markelin, L., Peltoniemi, J., Ahokas, E., Becker, S., 2006. Complete photogrammetric system calibration and evaluation in the Sjökulla test field -case study with DMC. EuroCOW, Castelldefels, Spain.

Honkavaara, E., Markelin, L., Ilves, R., Savolainen, P., Vilhomaa, J., Ahokas, E., Jaakkola, J., Kaartinen, H., 2005. In-flight Performance Evaluation of Digital Photogrammetric Sensors. ISPRS Workshop: High-Resolution Earth Imaging for Geospatial Information, Hannover, Germany.

Jahn, H. and Reulke, R., 1995. *Systemtheoretische Grundlagen optoelektronischer Sensoren*. Akademie Verlag, Berlin, Germany.

Leberl, F., Perko, R., Gruber, M., Ponticelli, M., 2003. The UltraCam Large Format Aerial Digital Camera System. Proceedings ASPRS, Annual Convention, Anchorage, on CD.

Pohl, C., van Genderen, J.L., 1998. Multisensor Image Fusion in Remote Sensing: Concepts, Methods and Applications. *International Journal of Remote Sensing*, Vol. 19, No. 5, pp. 823-854.

Reulke, R., Becker, S., Haala, N. & Tempelmann, U., 2006. Determination and improvement of spatial resolution of the CCD-line-scanner system ADS40. *ISPRS Journal of Photogrammetry and Remote Sensing* **60**(2), pp.81-90.

Saleh, B. E. A., Rabbani, M., 1983. Restoration of bilinearly distorted images: I. Finite impulse response linear digital filtering. *Journal of the Optical Society of America*, Vol. 73, pp. 66-70.

Sandau, R., Braunecker, B., Driescher, H., Eckardt, A., Hilbert, S., Hutton, J., Kirchhofer, W., Lithopoulos, E., Reulke, R., Wicki, S., 2000. Design Principles of the LH Systems ADS40 Airborne Digital Sensor. *IAPRS*, Vol.31 Part B1, pp.258-265.

Vrabel, J., 1996. Multispectral Imagery Band Sharpening Study. *Photogrammetric Engineering and Remote Sensing*, Vol. 62, No. 9, pp. 1075-1083.

Zhang, Y., 2002. Problems in the Fusion of Commercial High-Resolution Satellite Images as well as Landsat 7 Images and Initial Solutions. *IAPRS*, Vol. 34, Part 4.